Accepted for publication in the Astrophysical Journal
Preprint typeset using LaTeX style emulateapj v. 04/03/99

arXiv:astro-ph/0008404v1 25 Aug 2000

BROAD-BAND SPECTRAL ENERGY DISTRIBUTIONS OF ACTIVE GALACTIC NUCLEI FROM AN ACCRETION DISK WITH ADVECTIVE CORONAL FLOW

Toshihiro Kawaguchi[1,2], Toshiya Shimura[3], and Shin Mineshige[1]
[1]: Department of Astronomy, Graduate School of Science, Kyoto University, Sakyo-ku, Kyoto 606-8502, Japan
[2]: Research Fellow of the Japan Society for the Promotion of Science
[3]: International Graduate School of Social Sciences, Yokohama National University, Hodogaya-ku, Yokohama, 240-8501, Japan
e-mail: kawaguti@kusastro.kyoto-u.ac.jp
Accepted for publication in the Astrophysical Journal

ABSTRACT

Recent multi-waveband observations of Seyfert nuclei and QSOs established significant deviations in the spectral shape of the big blue bump from a blackbody one; Soft X-ray excess has a spectral index α ($F_\nu \propto \nu^{-\alpha}$) of 1.6 and hard X-ray tail with α of ~ 0.7. We construct a disk-corona model which accounts for such broad-band spectral properties. We study emission spectrum emerging from a vertical disk-corona structure composed of two-temperature plasma by solving hydrostatic equilibrium and radiative transfer self-consistently. A fraction f of viscous heating due to mass accretion is assumed to be dissipated in a corona with a Thomson optical depth of $\tau_{\rm c}$, where advective cooling is also included, and a remaining fraction, $1-f$, dissipates within a main body of the disk. Our model can nicely reproduce the soft X-ray excess with a power-law shape and the hard tail extending to ~ 50 keV. The different spectral slopes ($\alpha \sim 1.5$ below 2keV and ~ 0.5 above) are the results of different emission mechanisms and different sites; the former slope is due to unsaturated Comptonization from the innermost zone and the latter is due to a combination of the Comptonization, bremsstrahlung and a reflection of the coronal radiation at the disk-corona boundary from the inner to surrounding zone (≤ 300 Schwarzschild radii). The emergent optical spectrum is redder ($\alpha \sim 0.3$) than that of the standard disk ($\alpha \sim -0.3$), being consistent with observations, due to the different efficiencies of spectral distortion of disk emission at different radii. Further, we find that the cut-off frequency of the hard X-ray ($\sim$ coronal electron temperature) and broad-band spectral shape are insensitive to the black-hole mass, while the peak frequency of the big blue bump is sensitive to the mass as the peak frequency $\propto {M_{\rm BH}}^{-1/4}$.

Subject headings: accretion, accretion disks — black hole physics — galaxies: active — galaxies: nuclei — radiation mechanisms: miscellaneous

1. INTRODUCTION

Active Galactic Nuclei (AGNs) exhibit a lot of spectral components over a wide waveband; optical/ultraviolet (UV) bump, power-law component in hard X-rays, excess component in soft X-ray band (so called soft excess), warm absorber feature around 1 keV in some objects, and reflection/Fe Kα fluorescence line around a few to a few tens of keV (Mushotzky, Done & Pounds 1993; Koratkar & Blaes 1999 for reviews). Those spectral components are commonly thought to be powered by gas accretion onto a massive black hole. The most well-known disk-accretion model is called as the standard disk model (Shakura & Sunyaev 1973). According to the standard disk model, the spectrum at each radius of the disk is assumed to be a blackbody radiation with a local effective temperature, $T_{\rm eff}$. This simple picture was supported by their luminosity and by rough agreement of optical/UV spectral energy distribution (SED) between observations and models (e.g., Shields 1978; Malkan & Sargent 1982).

The standard model, however, has limitations; (i) if UV turn-over around 2000 Å is indeed an indication of the temperature at the innermost radius (e.g., Malkan 1983; Sun & Malkan 1989) such disks are too cool to produce enough soft X-ray photons. (ii) Inversely, if the soft excess component at 0.1 to 1 keV is due to radiation from the innermost region, as is often interpreted, such a disk only produces by 1.5–2 orders of magnitude less optical/UV flux than what is observed. (iii) When optical and soft X-rays spectra are simultaneously fitted with the disk spectrum, the luminosity of the disks (L) often exceeds the Eddington luminosity ($L_{\rm Edd}$). (iv) Observed optical spectra of QSOs are typically redder ($\alpha \sim 0.3$, where $L_\nu \propto \nu^{-\alpha}$; Francis et al. 1991) than those of the simplest standard accretion disks ($\alpha \sim -1/3$). In other words, a successful model spectrum of AGNs should deviate from that of the standard accretion disk. (v) Hard power-law X-ray cannot be reproduced.

Then, a number of authors have tried to distort the disk spectrum toward the high energy regime so that the disk can emit substantial soft X-ray and optical/UV radiation simultaneously. One promising idea is the Comptonization within the disk in the vertical direction (Czerny & Elvis 1987; Wandel & Petrosian 1988; Laor & Netzer 1989; Ross, Fabian & Mineshige 1992). The most accurate treatment of Comptonization in the framework of the standard model was made by Shimura & Takahara (1993, hereafter ST93) who solved radiative transfer and vertical structure simultaneously and

presented emergent spectra integrated over radii (see also Shimura & Takahara 1995, hereafter ST95). The effect of Comptonization is more prominent at higher accretion rates (e.g., Ross et al. 1992; ST93; ST95).

However, there still remain discrepancies between models and observations. (i) Although Comptonization tends to increase α, the Far-UV (FUV) spectra of these accretion disks exhibits $\alpha \sim 1$ at best when the luminosity of the disk approaches the Eddington limit (Ross et al. 1992; ST95). On the other hand, the observations of distant quasars showed steeper FUV spectra ($\alpha \sim 1.8$ – 2.2, Zheng et al. 1997). (ii) The observed small spectral indices in soft X-ray ($\alpha \sim 1.4$ – 1.6; e.g., Walter & Fink 1993; Laor et al. 1997) are not achieved by any disk models (e.g., Nandra et al. 1995 for Mrk 841; Laor et al. 1997 for a sample of low-redshift QSOs), because the higher energy tail of those disk models is the superposition of Wien laws, thus exhibiting exponential roll-over. (iii) These accretion disks still cannot reproduce the hard X-rays. Then, hard X-ray emission should be treated as additional components in these models.

With these problems kept in mind, we, in this present study, aim to produce the overall SED simultaneously by disk-corona models. The spectrum to be reproduced with these models is a composite one obtained from several independent observations (see Zheng et al. 1997; Laor et al. 1997). It is composed of 'typical' spectral indices over broad-bands from Near-IR to hard X-ray, optical–to–X-ray flux ratio, and the energy cut-off of the hard power-law component (see §3.1 for more detailed description). We can, for the first time, reproduce such broad-band spectra. In §2 we review the assumptions and numerical method used in the calculation. Numerical results and comparisons between the models and the composite spectrum are presented in §3. The final section is devoted to discussion and summary.

2. BASIC ASSUMPTIONS AND EQUATIONS

The numerical code used in this study is basically the same as that of ST93 except for some modifications. We assume for the configuration of the system that the accretion disk main body is sandwiched between coronal layers in the vertical direction (e.g., Haardt & Maraschi 1991), and that the whole system is geometrically thin (i.e., plane-parallel slab geometry). We treat the disk-corona system consisting of fully ionized hydrogen, thermal plasma around a Schwarzschild black hole of mass $M_{\rm BH}$. Gas evaporation from the disk to corona and -condensation from corona to disk (e.g., Meyer & Meyer-Hofmeister 1994) are not included here for simplicity; the disk and coronal layers are interacting only via radiation and pressure (e.g., Nakamura & Osaki 1993; Życki, Collin-Souffrin & Czerny 1995). Although magnetic fields may also affect the disk-corona structures, they are not included in this calculations.

The equation of hydrostatic equilibrium in the vertical direction is given by

$$-\frac{dP_{\rm gas}}{dz}+\int_0^\infty d\nu\frac{F_\nu}{\lambda_\nu c}=m_{\rm p}N_{\rm e}\frac{GM_{\rm BH}}{R^3}z, \tag{1}$$

where R and z are the radial and the vertical coordinates, respectively; and $P_{\rm gas}$ and $N_{\rm e}$ are the gas pressure and the number density of electrons, respectively. For the radiation field, we adopt the diffusion approximation. Then, the radiative flux F_ν at some frequency ν is given by

$$F_\nu=-\frac{c\lambda_\nu}{3}\left(\frac{\partial\epsilon_\nu}{\partial z}\right), \tag{2}$$

where ϵ_ν and λ_ν are the radiation-energy density per unit frequency per unit volume and the mean free path of a photon with a frequency ν, respectively. We set $\lambda_\nu=(\sigma_{\rm T}+\sigma_{{\rm ff},\nu})^{-1}N_e^{-1}$; we do not include the bound-free nor free-bound transitions in the calculations. Here, $\sigma_{\rm T}$ and $\sigma_{{\rm ff},\nu}$ are the cross sections of Thomson scattering and bremsstrahlung absorption, respectively. The Thomson optical depth of the disk-corona measured from the mid-plane τ is related to the height from the mid-plane z, as

$$d\tau=N_e\,\sigma_{\rm T}\,dz. \tag{3}$$

The total Thomson optical depth from the mid-plane (through the boundary between the disk-corona) to the surface of the corona, τ_0, is a free parameter. The equation of state is that $P_{\rm gas}=N_e k_{\rm B}(T_p+T_e)$, where T_p and T_e are temperature of protons and electrons, respectively.

The dissipated energy per unit surface area of the disk-corona system Q_0^+ in Newtonian approximation is written as (Shakura & Sunyaev 1973)

$$Q_0^+=\frac{3}{8\pi}\dot{M}{\Omega_{\rm K}}^2\left(1-\sqrt{3R_{\rm g}/R}\right), \tag{4}$$

where $\dot{M}$ and $\Omega_{\rm K}$ [$=(GM_{\rm BH}/R^3)^{1/2}$] are the total (above and below the mid-plane) accretion rate and the Keplerian angular velocity, respectively. The innermost radius of the disk-corona is assumed to be $3R_{\rm g}$, where $R_{\rm g}$ [$=2GM_{\rm BH}/c^2=3\times10^{13}{\rm cm}(M_{\rm BH}/10^8M_\odot))=0.01\,{\rm lt\text{-}day}\,(M_{\rm BH}/10^8M_\odot)$] is the Schwarzschild radius. For the case of a non-rotating black hole under non-relativistic treatment, $\dot{M}=12L_{\rm Edd}/c^2$ [$=2.6\,M_\odot{\rm yr}^{-1}(M_{\rm BH}/10^8M_\odot)$] corresponds to the accretion disk shining at $L_{\rm Edd}$ [$=1.3\times10^{46}{\rm erg\ sec}^{-1}(M_{\rm BH}/10^8M_\odot)$].

A constant fraction f of mass accretion is assumed to be dissipated in the corona with a Thomson optical depth of $\tau_{\rm c}$, where advective energy transport of protons is also included in addition to radiative cooling of electrons (see Figure 1).

A remaining fraction, $1-f$, dissipates within the disk layer. Advection in the disk layer (i.e., slim disk model that will be discussed later) is not included because of small radial velocity there. The advective cooling rate in the corona per unit surface area, $Q^-_{\rm adv}$, is taken from the expression of optically-thin advection dominated accretion flow (ADAF) in one-temperature case (i.e., $T_{\rm p}=T_{\rm e}$; see, Kato, Fukue & Mineshige 1998, p272):

$$Q^-_{\rm adv}=\frac{1}{16\pi^2}\left(\frac{\Omega_{\rm K}}{R^2}\right)\frac{(f\dot{M})^2\sigma_{\rm T}}{\alpha_c m_p \tau_c}. \tag{5}$$

Here, α_c is the viscosity parameter which controls the efficiency of the advection in the corona. We perform numerical calculations under the condition that the advective cooling should be less than the dissipated energy in the coronal layer; $Q^-_{\rm adv}\le f\ Q^+_0$.

The heating rate in the disk and corona, $q^+_{\rm d}$ and $q^+_{\rm c}$, respectively, and advective cooling rate in the corona per unit volume, $q^-_{\rm adv}$, are assumed to be proportional to matter density at each site. As a result, the fraction of advective cooling in the dissipated energy is

$$\frac{q^-_{\rm adv}}{q^+_{\rm c}}=\frac{Q^-_{\rm adv}}{f\,Q^+_0}=0.21\frac{f}{\alpha_c\tau_{\rm c}}\left(\frac{\dot{M}}{L_{\rm Edd}/c^2}\right)\left(\frac{R}{5R_{\rm g}}\right)^{-1/2}\left(1-\sqrt{\frac{3R_{\rm g}}{R}}\right)^{-1}. \tag{6}$$

The energy balance in each layer is as follows:

$$\text{Disk}: \ \text{Protons}: \quad q^+_{\rm d}=\lambda_{\rm ie} \tag{7}$$
$$\text{Electrons}: \quad \lambda_{\rm ie}=q^-_{\rm rad} \tag{8}$$
$$\text{Corona}: \ \text{Protons}: \quad q^+_{\rm c}=q^-_{\rm adv}+\lambda_{\rm ie} \tag{9}$$
$$\text{Electrons}: \quad \lambda_{\rm ie}=q^-_{\rm rad}, \tag{10}$$

with

$$q^+_{\rm d}=(1-f)Q^+_0\frac{\sigma_{\rm T}N_e}{\tau_0-\tau_{\rm c}},\qquad q^+_{\rm c}=fQ^+_0\frac{\sigma_{\rm T}N_e}{\tau_{\rm c}},\qquad q^-_{\rm adv}=Q^-_{\rm adv}\frac{\sigma_{\rm T}N_e}{\tau_{\rm c}}, \tag{11}$$

where $\lambda_{\rm ie}$ is the energy exchange rate due to Coulomb collisions taken from Guilbert and Stepney (1985); and $q^-_{\rm rad}$ is the radiative cooling rate. We consider bremsstrahlung and Comptonization for emission mechanisms. Then, radiative cooling rate $q^-_{\rm rad}$ is described as

$$q^-_{\rm rad}=\int d\nu(-cN_e\sigma_{{\rm ff},\nu}\epsilon_\nu+j_{{\rm ff},\nu}+j_{{\rm Comp},\nu}), \tag{12}$$

where $j_{{\rm ff},\nu}$ and $j_{{\rm Comp},\nu}$ are the bremsstrahlung emissivity (Rybicki & Lightman 1979) and the net rate of energy transfer from electrons to photons via Comptonization per unit volume per unit frequency, respectively. The latter is described by the Kompaneets equation (Rybicki & Lightman 1979; see Hua & Titarchuk 1995 for comparisons of the analytical treatment of Comptonization with Monte Carlo simulations). Thus, the radiative transfer equation for F_ν is written as

$$\frac{\partial F_\nu}{\partial z}=-cN_e\sigma_{{\rm ff},\nu}\epsilon_\nu+j_{{\rm ff},\nu}+j_{{\rm Comp},\nu}. \tag{13}$$

For the expression of the free-free absorption and emission ($\sigma_{{\rm ff},\nu}$ and $j_{{\rm ff},\nu}$, respectively), we take the Gaunt factor to be unity, for simplicity (see Rybicki & Lightman 1979).

Following ST93, we take $\xi\ [\equiv\log(\tau_0-\tau)\,]$ as an independent variable for the vertical coordinate. To calculate the spectra integrated over the whole disk (§3.1), we divide the disk-corona from $3R_{\rm g}$ to $300R_{\rm g}$ into 20 consentric rings so that each ring radiates approximately the same luminosity (cf. Ross et al. 1992; ST95). In total, input free parameters required for the calculations are $M_{\rm BH}$, $\dot{M}$, f, $\tau_{\rm c}$, τ_0, and α_c. The number of these parameters is similar to that of relevant observed parameters which we aim to explain simultaneously; e.g., L_X, $\alpha_{\rm ox}$, $\alpha_{\rm UV}$, $\alpha_{\rm opt}$, α_{ROSAT}, α_{ASCA}, etc. Then, outputs are $N_e(\xi)$, $T_e(\xi)$, $T_i(\xi)$, $P_{\rm gas}(\xi)$, $z(\xi)$, and $\epsilon_\nu(\xi)$. Spectrum of the whole disk-corona system is obtained by summing up the emergent spectra of all the rings.

The emergent spectrum at each ring does not so strongly depend on τ_0 as long as $\tau_0\gg1$, but is sensitive to $\tau_{\rm c}$. We, thus, take τ_0 as a constant over all rings, for simplicity. Currently, we do not have a good theory to predict the radial dependence of $\tau_{\rm c}$ and f that can, in principle, be determined by physics of evaporation/condensation. Thus, $\tau_{\rm c}$ and f are also simply assumed to be constant over all rings. The effects of changing $\tau_{\rm c}$ and f will be discussed later.

General relativistic effect is not included. Since no Doppler broadening is considered, the total spectrum represents the case of a face-on disk. Convection/conductive energy transport is not included. Shakura, Sunyaev & Zilitinkevich (1978) have shown that convection transports no more than ~30 % of the vertical energy flux.

3. SPECTRAL ENERGY DISTRIBUTION OF AGNS

3.1. *Observed Composite Spectrum*

The spectrum to be reproduced with our models is a composite one (dotted lines in Figure 2a), which is a useful probe to see whether a model for the SED of AGNs can work or not. The vertical normalization is determined so as to give rise to a representative optical luminosity among low-redshift quasars from the Bright Quasar Survey adopting H_0 of 50 km s^{-1} Mpc^{-1} and q_0 of 0.5 with an assumption of isotropic emission (see Laor et al. 1997). There are, however, two major problems that one should keep in mind when dealing with the composite spectrum (Koratkar & Blaes 1999; Laor 1999). (i) We observe objects with different redshifts in different wavebands; spectral index in FUV is obtained from distant QSOs (Zheng et al. 1997), while that of soft X-ray is mainly from nearby objects (e.g., Walter & Fink 1993; Laor et al. 1997). Also, sample used in each wavebands contains objects that are not necessarily the same objects. (ii) Soft excess might be an instrumental/calibration problem; *BeppoSAX* observations did not detect soft X-ray excess in some objects while excess was seen for the same objects with other telescopes (e.g., Matt 1999). Although the results are still controversial, we assume that soft excess really exists in most AGNs throughout this paper. In what follows, we try to reproduce broad-band spectra similar to the composite one, as the first step.

3.2. *Model Spectrum Integrated over Radii*

We first show the most successful case with $M_{\rm BH} = 3 \times 10^9 M_\odot$ and $\dot{M} = 0.5\ L_{\rm Edd}/c^2$ that gives rise to luminosity of about 5 % of the Eddington limit for a non-rotating black hole under non-relativistic treatment. Thick line in figure 2a shows an example of the resultant broad-band spectra. Since the innermost ring from 3.0 $R_{\rm g}$ to 4.0 $R_{\rm g}$ does not satisfy the restriction that $q^-_{\rm adv}/q^+_{\rm c} \leq 1.0$ for the parameter sets described in Fig. 2a, we, hereafter, plot integrated spectra from 4.0 $R_{\rm g}$ to 300 $R_{\rm g}$. In other words, all dissipated energy is assumed to be carried out by advection in $3.0 < R < 4.0 R_{\rm g}$. To account for the radiation at the surfaces of coronae above and beyond the disk, the resultant spectrum is multiplied by two. A significant fraction $f = 0.6$ of mass accretion occurs at the corona. In this case, advective cooling in the corona is comparable with the radiative cooling at $R \sim 4.9 R_{\rm g}$; $q^-_{\rm adv}/q^+_{\rm c} \sim 0.5$ [eq. (6)]. A spectrum of the standard disk with the same $M_{\rm BH}$ and $\dot{M}$ is also depicted for comparison (dashed line).

Presence of multiple spectral components is the most noteworthy feature of the present model. This is because different radiative mechanisms play roles in different wavebands in Fig. 2a; thermal radiation of the disk in optical/UV, unsaturated Comptonization in FUV/soft X-ray, and a combination of the power-law component due to Comptonization, bremsstrahlung, and a reflection in hard X-ray. Note that the underlying radiative processes in soft–hard X-rays are distinct from those of the traditional explanation, in which UV–soft X-ray component is due to blackbody whereas hard power-law component is due to Comptonization of the soft photons. In our model, hard X-ray spectrum looks a power-law with $\alpha \sim 0.5$–1.0 due to the combination of multiple radiative mechanisms, in contrast.

Figure 2b shows contributions to the total spectrum ($4.0 R_{\rm g} < R < 300 R_{\rm g}$; thick line) due to individual rings. The outermost ring ($104 R_{\rm g} < R < 300 R_{\rm g}$) contribute as much as one third of the total spectrum at a few tens of keV. Usual models for X-ray emission of AGNs assume that only inner region radiates X-ray (i.e., one-zone); our model differs from the traditional model in terms of radial dependence of the X-ray spctrum, as well. Like optically-thin ADAF (e.g., Narayan, Yi & Mahadevan 1995; Manmoto, Mineshige & Kusunose, 1997), X-ray emission arises from wide spatial range ($R \lesssim 300 R_{\rm g}$), in contrast with a usual belief. Interestingly, contribution from the outer rings to the total X-ray spectrum decreases towards lower-energy X-ray band. Provided that inner rings are more time-variable than outer rings, resultant X-ray spectrum will get softer when the luminosity increases, as is actually observed (e.g., Done et al. 1995; Leighly et al. 1996). The most powerful test of our model will be gravitational microlensing (Yonehara et al. 1998) which provides information as to the size of emission region as a function of wavelength on AU ($\sim R_{\rm g}$ for $10^8 M_{\rm BH}$) scales.

The effect of advective cooling in the coronal layer to the emergent spectrum is demonstrated in Figure 2c. Thick dashed line is the resultant spectrum without advective cooling, which corresponds to a two-temperature treatment of the study by Shimura, Mineshige, & Takahara (1995), but with a constant $\tau_{\rm c}$. Lower dashed curves represents the spectra of each ring in the case without advective cooling. Thick solid curve has the same meaning as in Fig. 2a and 2b.

In our models above (Fig. 2a–2c), we assumed constant f and $\tau_{\rm c}$ over all rings. This will be a reasonable assumption since Janiuk, Życki & Czerny (2000), for example, estimated f as a function of radius under some assumptions, finding that f is a slowly increasing variable with radius, and that $0.2 < f < 1.0$ for various parameter sets at 3 to 300 $R_{\rm g}$. The coronal gas is probably originated in evaporated gas cumulated in the flow (Meyer & Meyer-Hofmeister 1994; Liu, Meyer & Meyer-Hofmeister 1997). In other words, we have assumed that a disk corona has already formed until $\sim 300\ R_{\rm g}$. If, however, evaporation of disk material is still active at $R \lesssim 300 R_{\rm g}$, $\tau_{\rm c}$ and f are both likely to increase with a decreasing radius. To what extent the resultant spectrum changes in such a case is demonstarated in figure 2d. Spectra for the outermost ring with $f = \tau_{\rm c} = 0.6$ (solid curve) and $f = \tau_{\rm c} = 0.1$ (dashed curve) are shown. In the latter case, hard X-ray emission is not strong as the former case, in which bremsstrahlung emission at the outermost ring is the main origin of hardening in the total X-ray spectrum (thick solid curve). Then, we are lead to the conclusion that the corona must have developed until $300 R_{\rm g}$ so as to have large values of f and $\tau_{\rm c}$ at the outermost ring, thereby reproducing the observed spectrum.

3.3. *Red Optical Spectrum*

Optical spectral index of QSOs has been recognized as a discrepancy between disk models and observations; Francis et al. (1991) reported that the bright QSOs, in which stellar contamination to the optical fluxes is relatively negligible, typically show spectral index in optical, α at 1500–5000 Å, of 0.32 ($L_\nu \propto \nu^{-\alpha}$), while the classical standard disk model predict that of -0.33 (i.e., $L_\nu \propto \nu^{1/3}$).

In order to emphasize the optical spectra, a part of Fig. 2a is enlarged and shown in figure 3 with additional spectra of disk models integrated over $3 < R < 1000R_g$. Thick solid and dotted lines have the same meanings as in Fig. 2a, and they both show similar spectral index, $\alpha \sim 0.3$. The shaded area inndicates the relevant waveband, 1500–5000 Å.

The reason why the current model has a better agreement with the observations in terms of the optical spectral index is as follows. The long-dashed line is a spectrum of the standard disk (i.e., eq. 4), but without the inner boundary term (the term within the parenthesis on the right-hand-side of eq. 4, which is sometimes omitted when roughly estimating the spectral index of the disk model). It shows $\alpha \sim -0.3$. Spectra of the standard disks with the inner boundary term are drawn by the short-dashed lines. The upper one represents the disk with $M_{\rm BH} = 3 \times 10^9 M_\odot$ and $\dot{M} = 0.5\, L_{\rm Edd}/c^2$, while the lower one is for $M_{\rm BH} = 10^8 M_\odot$ and $\dot{M} = L_{\rm Edd}/c^2$ showing somewhat redder spectrum ($\alpha \sim -0.1$) due to the inner-boundary term.

The emergent local spectrum changes its shape in a sense that the spectrum is distorted and shifted towards shorter wavelength when the electron scattering in the disk is taken into account (Czerny & Elvis 1987). Such a spectral shift is more efficient in inner region than in outer region. As the result, disk models with electron scattering finally show redder optical spectra, $\alpha \sim +0.1$ in lower solid curve and $\alpha \sim +0.3$ in upper solid curve. The difference of spectral indices in the two solid curves, which are obtained by radial integrations of ST93 model (i.e., no corona), are due mainly to the difference of their black-hole masses. The disk with larger $M_{\rm BH}$ gets cooler at fixed $\dot{M}/L_{\rm Edd}$ and R/R_g, as is expected for the standard accretion disk (eq. 14 described later). The optical band becomes to measure the flux at inner part of the disk, where it gets close to the edge of the integral interval (e.g., $3 < R < 1000R_g$). Then, the emergent spectrum is somewhat curved in a sense that it is redder than the spectrum from outer region (e.g., figure 16 in Koratkar & Blaes 1999). Note that the redder spectra are achieved even within the framework of original ST93 and ST95 models, as well as our disk-corona model. If one wants to discuss in more details about optical spectra, heavy metals, bound-bound, free-bound, bound-free transitions and precise estimation of the contribution from broad line region (e.g., Balmer continuum) must be included.

3.4. *Spectra for Various $M_{\rm BH}$ and $\dot{M}$*

Figure 4 shows the black-hole mass dependence of the spectra with a fixed ratio of $\dot{M}$ to $L_{\rm Edd}$ (i.e., fixed $\dot{M}/M_{\rm BH}$). The peak frequency of the big blue bump varies with $M_{\rm BH}$ in a similar fashion to that of the standard accretion disk in which

$$T_{\rm eff}(4R_{\rm g}) \propto {M_{\rm BH}}^{-1/2}\dot{M}^{1/4} \;\propto\; {M_{\rm BH}}^{-1/4}(\dot{M}/L_{\rm Edd})^{1/4}. \tag{14}$$

On the other hand, the cut-off frequency of the hard X-ray (i.e., coronal electron temperature) and the spectral slopes in X-rays are rather insensitive to the black-hole mass.

Accretion-rate dependence of the emergent spectra with a fixed blackhole mass ($M_{\rm BH} = 3 \times 10^9 M_\odot$) is shown in Figure 5. The spectral slope at 0.1 – 2.0 keV stays almost constant, $\alpha = 1.46$, 1.58, 1.62 for $\dot{M}/(L_{\rm Edd}/c^2) = 0.1$, 0.5 and 0.7, respectively.

3.5. *Vertical Structure*

We finally present the vertical structure of the disk/corona. Number density of electrons (dotted line) and temperature of protons (crosses) and electrons (solid line) at $R \sim 4.9R_{\rm g}$ are shown in Figure 6. The left side of the figure where ξ [$\equiv \log(\tau_0 - \tau)$] $= 3$ corresponds to the mid-plane (i.e., $\tau_0 = 1000$), and the boundary between the disk and corona is located at $\xi \sim -0.2$ (i.e., $\tau_{\rm c} = 0.6$). Parameters used here are the same as those of Fig. 2a. It turns out that the height of the boundary measured from the mid-plane is 0.03 $R_{\rm g}$, and that of the surface of the corona (at ξ of -2) is 0.3 $R_{\rm g}$. Then, the disk-corona system is indeed geometrically thin; the height of the corona from the mid-plane $\lesssim 0.1R$.

4. DISCUSSION AND CONCLUSION

4.1. *Comparison with previous models*

The most widely accepted interpretation, to date, of soft and hard X-ray emission mechanisms is that soft excess is due to unscattered photons propagating from the disk-corona boundary to the coronal surface, while hard power-law emission is attributed to unsaturated Comptonization, i.e., photons that are Compton up-scattered during the propagation within the corona. Monte-Carlo simulations of propagating photons in the framework of two zone treatment (disk and coronal layers) indeed reproduce bump-like feature in soft X-ray and power-law component due to Comptonization in hard X-ray (e.g., Haardt & Maraschi 1991; Nakamura & Osaki 1993). However, the bump-like feature due to unscattered photons still keeps its spectral shape as it was at the disk-corona boundary even after it goes away from the coronal surface: i.e., it should look like blackbody radiation. Then, higher energy tail of the soft excess is predicted to be as steep as the Wien law, in contradiction with observed small spectral indices in soft X-ray ($\alpha \sim 1.4$ – 1.6).

Thermal bremsstrahlung emission was proposed for hard X-ray power-law component by Schlosman, Shaham & Shaviv (1984), in which the emission comes from the disk-corona transition layer with an temperature gradient, where thermal conduction from the overlying corona is balanced with radiative cooling. They show that such a layer emits hard X-rays efficiently in the case of an accretion disk model proposed by Sakimoto & Coroniti (1981), in which viscous torque is proportional to gas pressure, but that it does not work in standard accretion disks where the torque is in proportion to the total pressure unless viscosity parameter in the disk is less than 10^{-3}. We should note here that non-thermal, power-law electron energy distribution models, similarly to our results, produce two spectral power-laws for soft and hard X-ray emissions (e.g., Zdziarski & Lightman 1985), although ours is a thermal model.

Shimura et al. (1995) proposed a model in which FUV–hard X-ray is attributed to unsaturated Comptonization in a corona above a disk. Their claim is that their model, with $\tau_{\rm c}$ being a strongly increasing function with increasing radius, reproduces a single power-law in X-ray bands, not a broken power-law (i.e., soft excess and hard power-law). Then, the corona could be patchy so that the disk is covered over only in part with the corona. In our model, however, bremsstrahlung emission from the corona and reflection of the coronal emission at the disk-corona boundary also contribute to hard X-ray as well as the unsaturated Comptonization. As a result, we have different spectral slopes at soft and hard X-ray bands. It largely depends on our assumption of constant f and $\tau_{\rm c}$. In other words, we need f and $\tau_{\rm c}$ to be almost constant or weak functions of radius in order to expect sufficient bremsstrahlung emission from the corona at outer region and then in order to reproduce the observed spectrum within the current framework. Theoretical works to check the assumption are needed as next steps. Without advective cooling in the corona, we also have rather straight spectrum from FUV to hard X-ray (see Fig. 2c). The effect of advection seems to bent the total spectrum so as that the spectrum has two power-laws in X-ray bands.

In the extremely high accretion rate, the disk spectra may be able to reproduce the observed steep spectral decline at 1000Å–400Å, since Comptonization is more efficient at higher accretion rates and since an increase of accretion rate changes the disk dynamics from the standard disk to optically-thick ADAF. Optically-thick ADAF, which is so called the slim disk model, radiates with higher temperature than the standard disk (Szuszkiewicz, Malkan & Abramowicz 1996; Mineshige et al. 2000). Narrow-Line Seyfert 1 galaxies (NLS1s) have peculiar spectral and temporal features that are not seen in normal Seyfert nuclei and QSOs (e.g., Boller, Brandt, & Fink 1996; Brandt, Mathur, & Elvis 1997; Leighly 1999a, 1999b; Grupe et al. 1998, 1999). These features are often attributed to small black-hole mass and to high accretion rate (i.e., $L \sim L_{\rm Edd}$; e.g., Pounds, Done, & Osborne 1996; Hayashida et al. 1998; Mineshige et al. 2000). Then, such extreme accretion rate is not relevant in this study, where we are going to construct a disk model for normal Seyferts/QSOs that perhaps have moderate accretion rate [$L \sim (0.01 - 0.1)$ of $L_{\rm Edd}$; e.g., Wandel 1999]. To account for systematically large α_{ROSAT} in NLS1s, we would need to reduce Compton-y parameter in the corona.

The configuration of cold ($\sim 10^5$ K) and hot (~ 100 keV) regions that radiate optical/UV bump and X-rays, respectively, is an unsolved problem. Optically-thin ADAF is a possible energy source of X-ray emissions. However, optically-thin ADAF itself is basically faint (e.g., Mahadevan 1997) compared with observed luminosity of AGNs. Then, the luminosity of the power-law X-ray emission indicates that cold material is located adjacent to such hot flow as a source of seed photons: for example, corona-like flows above and below a disk (e.g., Liang & Price 1977; Haardt & Maraschi 1991). Separation in the vertical direction has been also suggested from the stability against thermal and secular instabilities in inner, radiation-pressure dominated region of the disk (Ionson & Kuperus 1984; Nakamura & Osaki 1993; Mineshige & Kusunose 1993), the correlated variabilities between the iron-line flux and the X-ray continuum (e.g., Nandra et al. 1999; see also, however, Lee et al. 1999), and need for a cold disk as a 'mirror' for reflection-component/broad-fluorescence line (e.g., Tanaka et al. 1995; Mushotzky et al. 1995; Nandra et al. 1997). Another potential problem is that those layers could be inhomogeneous and highly time dependent; the corona can be patchy (Shimura, Mineshige, & Takahara 1995; Di Matteo 1998; Kawaguchi et al. 2000; Machida et al. 2000), or the cold gas may exist as numerous blobs within the corona instead of the slab geometry (Guilbert & Rees 1988; Lightman & White 1988; Sivron & Tsuruta 1993; Collin-Souffrin et al. 1996; Krolik 1998; Różańska 1999). Nevertheless, spatially and temporally averaged treatment of the cold and hot regions will still be useful for study of time-averaged spectrum. Appropriate treatment of mass evaporation/condensation process is another future issue. In other words, f and $\tau_{\rm c}$ may be variable in terms of R, $M_{\rm BH}$, $\dot{M}$, etc. For instance, see Janiuk et al. (2000) for f as a function of R with various $\dot{M}$ and viscosity parameter, and Życki et al. (1995) for $\tau_{\rm c}$ v.s. $\dot{M}$.

4.2. *Expected Time Variability*

Time variability provides strong constraints on spectral models. Then, it will be worthwhile to briefly comment on the temporal behaviour, although we are now working on a model for the steady accretion disk-corona with an aim to reproduce the observed, time-averaged spectrum. Followings are qualitative arguments expected from our current model. More details are out of the scope of this paper, and will be remained as future works.

For the optical-to-UV time-lag observed in NGC 7469 (Wanders et al. 1997; Collier et al. 1998) and marginally detected in NGC 4151 (Peterson et al. 1998), our model can explain the lag as Collier et al. (1998) demonstrated using the standard accretion disk model. That is because optical/UV emitter in our model is, like other spectral models, an accretion disk that has a similar dependence of (surface) temperature upon radius to the standard accretion disk. It should be noted here that such a time-lag has not yet been established in all AGNs (Edelson et al. 2000)

Since the FUV, soft X-ray and a part of hard X-ray emission come from the same region in our model, they are expected to vary without serious time-lag (larger than an order of days), except for difference of escaping (diffusion) time at different

energies. Chiang et al. (2000) reported the inter-band lags in NGC 5548 from $\sim$ 240 k sec simultaneous observations; 0.14-0.18 keV flux leads 0.78 keV flux by $\sim$ 10 k sec, and 5.4 keV flux by $\sim$ 30 k sec. As discussed in section 6 in their paper, these lags are consistent with a coronal size of 10 R_g for a $10^8 M_\odot$ black-hole. Incidentally, the blackhole mass of NGC 5548 is estimated to be about $10^8 M_\odot$ through the reverberation mapping method (Wandel, Peterson & Malkan 1999; Kaspi et al. 2000). However, the $\sim$ 4-day X-ray lag behind UV near the peak flux levels and almost simultaneous variations near the minimum fluxes detected in NGC 7469 (Nandra et al. 1998) is not solved by our model easily, as well as other models, to date, fail to do.

Finally, our model qualitatively explains following two issues about spectral variability in X-rays on short timescales (less than months) that are reported by numerous X-ray observations (§3.2). i) Soft X-ray flux is more variable than hard X-ray flux. ii) Hard X-ray becomes softer when it gets brighter.

4.3. *Conclusions*

We study emission spectrum emerging from the vertical disk-corona structure composed of two-temperature plasma by solving hydrostatic equilibrium and radiative transfer self-consistently. The key question is what physical condition exhibits a soft X-ray excess with a spectral index α ($F_\nu \propto \nu^{-\alpha}$) of 1.6 and a hard X-ray tail with α of 0.7 at the same time. In our model, a fraction f of viscous heating is assumed to be dissipated in a corona with a Thomson optical depth of $\tau_{\rm c}$, where advective cooling is also included, and a remaining fraction, $1-f$, dissipates within a main body of the disk. Our model can nicely reproduce the observed composite spectrum of AGNs, which shows soft X-ray excess with α of about 1.5 and hard tail extending to $\sim$ 50 keV with a different slope ($\alpha \sim 0.5$). Our model should be checked with individual objects in the future, though.

The broken power laws ($\alpha \sim 1.5$ below 2keV and ~ 0.5 above) are the results of different emission mechanisms: unsaturated Comptonization in soft X-rays and a combination of the Comptonization, bremsstrahlung, and a reflection of the coronal radiation at the disk-corona boundary in hard X-rays. Previous models, where soft X-ray excess is attributed to blackbody or saturated Comptonization of the disk blackbody, tended to deal with limited wavebands separately, while we tried to fit the broad-band SED simultaneously. That is the reason why we propose here emission mechanisms, that are different from previous models, in soft and hard X-ray bands. Also, our model differs from traditional models in terms of X-ray emitting region; hard X-ray emission causes from spatially spread region up to 300 Schwarzschild radii. The emergent optical spectrum is redder ($\alpha \sim 0.3$) than that of the standard disk ($\alpha \sim -0.3$), being consistent with observations, due to the different efficiencies of spectral distortion and shift of disk emission at different radii. The cut-off frequency of the hard X-ray (reflecting the coronal electron temperature) and X-ray spectral slopes are insensitive to the black-hole mass, while the peak frequency of the big blue bump is sensitive to the mass.

We wish to thank Hitoshi Negoro for helpful discussions and encouragement, Makoto Kishimoto, Masaru Matsuoka, Juri Poutanen, Ken Ebisawa and Lev Titarchuk for useful comments. We would also like to thank an anonymous referee for rewarding suggestions. T.K. appreciates the organizers of the Guillermo Haro Advanced Lectures on the starburst-AGN connection held in Mexico, 2000, for providing him the excellent lectures and acknowledges useful discussions with the participants, especially Dario Trevese and Agnieszka Janiuk. This work was supported in part by the Research Fellowship of the Japan Society for the Promotion of Science for Young Scientists (4616, TK), and by the Grants-in Aid of the Ministry of Education, Science, Sports and Culture of Japan (10640228, SM).

REFERENCES

Boller Th., Brandt W.N., Fink H.H. 1996, A&A 305, 53
Brandt W.N., Mathur S., Elvis M. 1997, MNRAS 285, L25
Chiang J. et al. 2000, ApJ, 528, 292
Collier, S. J., et al. 1998, ApJ, 500, 162
Collin-Souffrin S., Czerny B., Dumont A.-M., and Życki P.T. 1996, A&A, 314, 393
Czerny, B. & Elvis, M. 1987, ApJ, 321, 305
Di Matteo T. 1998, MNRAS, 299, L15
Done C., Pounds K.A., Nandra K. & Fabian A.C. 1995, MNRAS, 275, 417
Edelson R. et al. 2000 ApJ, 534, 180
Francis, P. J., Hewett, P. C., Foltz, C. B., Chaffee, F. H., Weymann, R. J., & Morris, S. L. 1991, ApJ, 373, 465
Grupe G.D., Beuermann K., Thomas H.-C., Mannheim K. Fink H.H. 1998, A&A 330, 25
Grupe G.D., Beuermann K., Mannheim K., Thomas H.-C. 1999, A&A 350, 805
Guilbert P. W. & Stepney S. 1985, MNRAS, 212, 523
Guilbert, P.W., & Rees, M.J. 1988, MNRAS, 233, 475
Haardt, F., & Maraschi, L. 1991, ApJ, 380, L51
Hayashida K. et al. 1998, ApJ 500, 642
Hua X.-M., & Titarchuk L. 1995, ApJ, 449, 188
Ionson J.A. & Kuperus M. 1984, ApJ, 284, 389
Janiuk A., Życki P.T., and Czerny B. 2000, MNRAS, 314, 364
Kaspi S., Smith P.S., Netzer H., Maoz D., Jannuzi B.T. & Giveon U. 2000, ApJ, 533, 631
Kato S., Fukue J., & Mineshige S. 1998, Black-Hole Accretion Disks, Kyoto Univ. Press
Kawaguchi T., Mineshige S., Machida M., Matsumoto R. & Shibata K. 2000, PASJ, 52, L1
Koratkar A. & Bales O. 1999, PASP, 111, 1
Krolik, J. H. 1998, ApJ, 498, L13
Laor, A., & Netzer, H. 1989, MNRAS, 238, 897
Laor A., Fiore F., Elvis M., Wikes B. J. & McDowell J. C. 1997, ApJ, 477, 93
Laor A. 1999, in Quasars and Cosmology. eds. G. Ferland & J. Baldwin ASP Conf. series
Lee J.C., Fabian A.C., Reynolds C.S., Brandt W.N., and Iwasawa K. 1999, astro-ph/9909239
Leighly K.M., Kunieda H., Awaki H. & Tsuruta S. 1996, ApJ, 463, 158
Leighly K.M. 1999a, ApJS, 125, 297
Leighly K.M. 1999b, ApJS, 125, 317
Liang E.P.T. & Price R.H. 1977, ApJ, 218, 247
Lightman, A.P., & White, T.R. 1988, ApJ, 335, 738
Liu B.F., Meyer F. & Meyer-Hofmeister E. 1997, A&A, 328, 247
Machida M., Hayashi M. & Matsumoto R. 2000, ApJ, 532, L67
Mahadevan R. 1997, ApJ, 477, 585
Malkan, M., A., & Sargent, W. L. W. 1982, ApJ, 254, 22
Malkan, M., A. 1983, ApJ, 268, 582
Manmoto, T., Mineshige, S., & Kusunose, M. 1997, ApJ, 489, 791
Matt, G. 1999, in High Energy Processes in Accreting Black Holes, eds. J. Poutanen & R. Svensson, ASP Conf. Series
Meyer, F., & Meyer-Hofmeister, E., 1994, A&A, 288, 175
Mineshige S., Kawaguchi T., Takeuchi M. & Hayashida K. 2000, PASJ, 52, 499
Mineshige S. & Kusunose M. 1993, PASJ, 45, 113

Mushotzky, R. F., Done, C., & Pounds, K. A. 1993, ARA&A, 31, 717
Mushotzky, R. F., Fabian, A. C., Iwasawa, K., Kunieda, H., Matusoka, M., Nandra, K., & Tanaka, Y. 1995, MNRAS, 272, L9
Nakamura, K., & Osaki, Y. 1993, PASJ, 45, 775
Nandra, K., Turner, T.J., George, I.M., Fabian, A.C, Shrader C., & Sun, W.-H. 1995, MNRAS, 273, 85
Nandra, K., George, I. M., Mushotzky, R. F., Turner, T. J., & Yaqoob, T. 1997, ApJ, 477, 602
Nandra, K., George, I. M., Mushotzky, R. F., Turner, T. J., & Yaqoob, T. 1999, ApJ, 523, L17
Narayan, R., Yi, I., & Mahadevan, R. 1995, Nature, 374, 623
Peterson, B. M., Wanders, I., Horne, K., Collier, S., Tal, A., Kaspi, S., & Maoz, D. 1998, PASP, 110, 660
Pounds K.A., Done C., Osborne J. 1996, MNRAS 277, L5
Ross, R. R., Fabian, A. C., & Mineshige, S. 1992, MNRAS, 258, 189
Różańska A. 1999 MNRAS, 308, 751
Rybicki, G. B., & Lightman, A. P. 1979, Radiative Processes in Astrophysics, John Willey & Sons, New York
Sakimoto P.J. & Coroniti F.V. 1981, ApJ, 247, 19
Schlosman I., Shaham J., & Shaviv G. 1984, ApJ, 287, 534
Shakura N.I. & Sunyaev R.A., 1973, A&A, 24, 337
Shakura N.I., Sunyaev R.A., & Zilitinkevich S.S. 1978, A&A, 62, 179
Shields, G., A. 1978, Nature, 272, 706
Shimura, T,, Mineshige, S., & Takahara, F. 1995, ApJ, 439, 74
Shimura, T., & Takahara, F. 1993, ApJ, 419, 78 (ST93)
Shimura, T., & Takahara, F. 1995, ApJ, 440, 610 (ST95)
Sivron R., & Tsuruta, S. 1993, ApJ, 402, 420
Sun, W.-H., & Malkan, M. A. 1989, ApJ, 346, 68
Szuszkiewicz, E., Malkan, M. A., & Abramowicz, M. A. 1996, ApJ, 458, 474
Tanaka, Y., et al. 1995, Nature, 375, 659
Walter R. & Fink H. H. 1993, A&A, 274, 105
Wandel A., Peterson B.M. & Malkan M.A. 1999, ApJ, 526, 579
Wandel A. & Petrosian V. 1988, ApJ, 329, L11
Wandel A. 1999, ApJ, 527, 649
Wanders, I., et al. 1997, ApJS, 113, 69
Życki P.T., Collin-Souffrin S., and Czerny B. 1995, MNRAS, 277, 70
Zheng, W. Kriss, G. A., Telfer, R. C., Grimes, J. P., & Davidsen, A. F. 1997, ApJ, 475, 469
Yonehara, A., Mineshige, S., Manmoto, T., Fukue, J., Umemura, M., & Turner, E. L. 1998, ApJ, 501, L41
Zdziarski, A. A., & Lightman A. P. 1985, ApJ, 294, L79

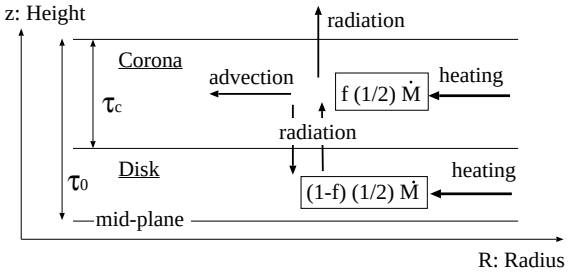

FIG. 1.— A schematic view of the energy balance in the present model.

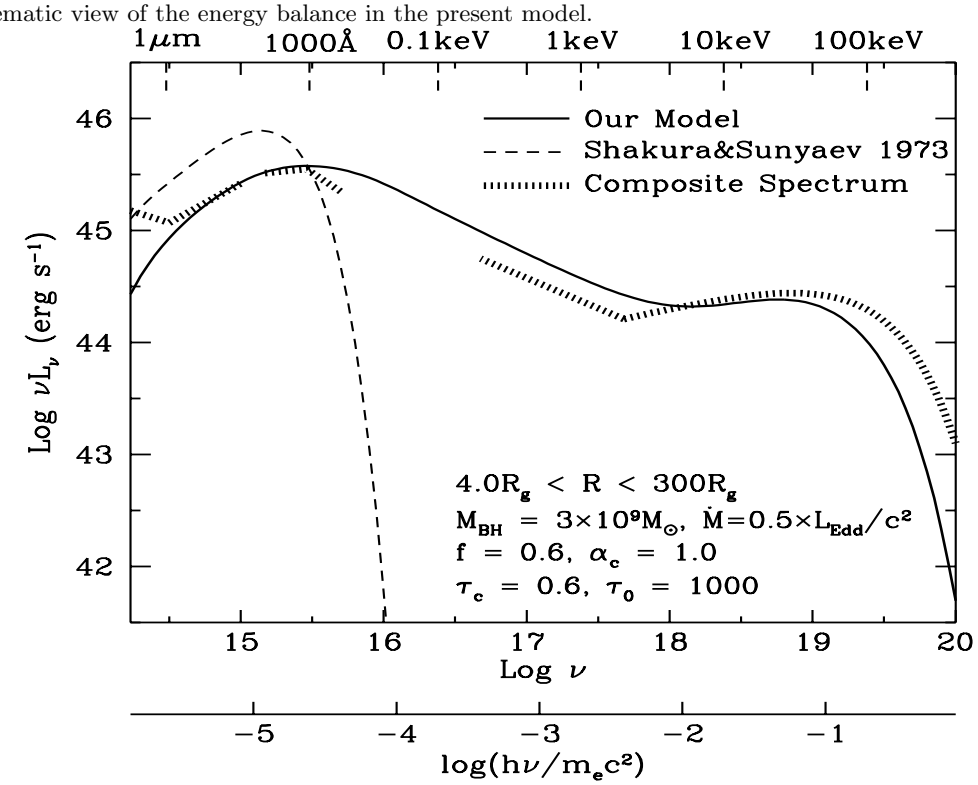

FIG. 2a.— Resultant spectrum from the disk-corona structure integrated over 4.0 to $300R_{\rm g}$ (thick line). Parameters used in this model are listed in the figure. With those parameter sets, advective cooling in the corona is comparable with the radiative cooling at $R \sim 4.9R_{\rm g}$; $q^{-}_{\rm adv}/q^{+}_{\rm c} \sim 0.5$. Dashed line indicates the integrated spectra of the standard disk with the same $M_{\rm BH}$ and $\dot{M}$. Spectral indices of the observed composite spectra (dotted lines) are: α of 1.4 at NIR ($\lambda \geq 1\mu m$), 0.3 at optical ($1\mu m \geq \lambda \geq 2500$Å), 1.0 at UV (2500Å $\geq \lambda \geq$ 1000Å), 1.8 at FUV (1000Å $\geq \lambda$), 1.6 at soft X-ray (0.2–2.0 keV), 0.7 at hard X-ray (> 2.0keV), 1.5 between optical and X-ray (2500 Å–2keV). The energy cut-off for the hard X-ray power-law is assumed to be 100 keV.

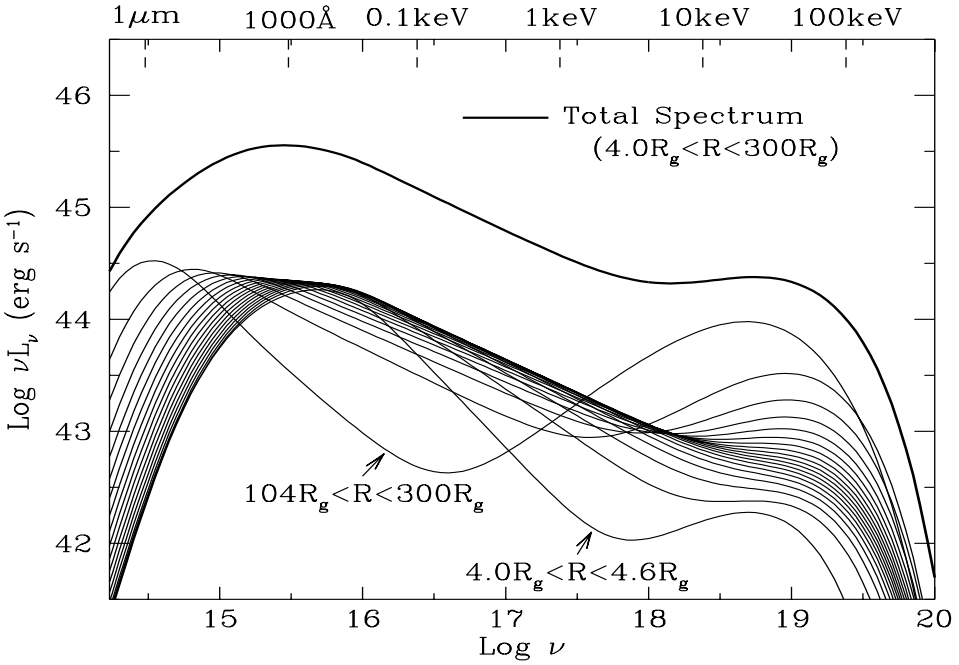

FIG. 2b.— Contributions to the total spectrum due to individual rings (lower curves). Thick line denotes the total spectrum ($4.0R_{\rm g} < R < 300R_{\rm g}$) as the same as in Fig. 2a.

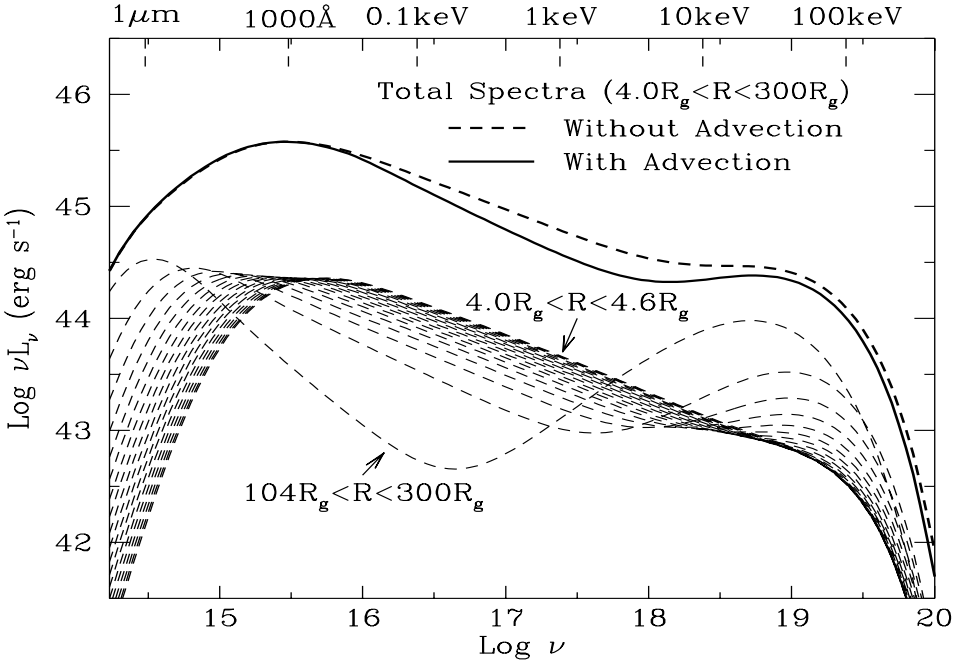

FIG. 2c.— The effect of advective cooling in the corona layer to the emergent spectrum. Thick dashed line is the resultant spectrum without advective cooling. Lower dashed curves represents contributions to the total spectrum due to each ring. Thick solid curve has the same meaning as in Fig. 2a and 2b.

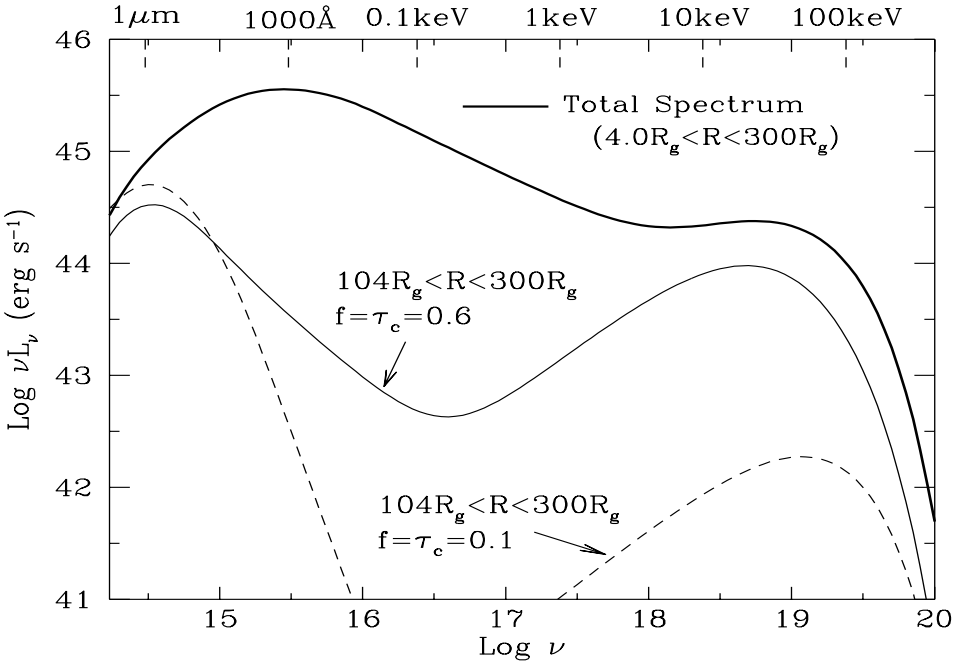

FIG. 2d.— Spectra for the outermost ring with $f = \tau_c = 0.6$ (solid curve) and $f = \tau_c = 0.1$ (dashed curve). It is shown that hard X-ray emission in the latter case is not strong as the former case, where bremsstrahlung emission at the outermost ring is the main origin of hardening in the total X-ray spectrum (thick solid curve; see Fig. 2b).

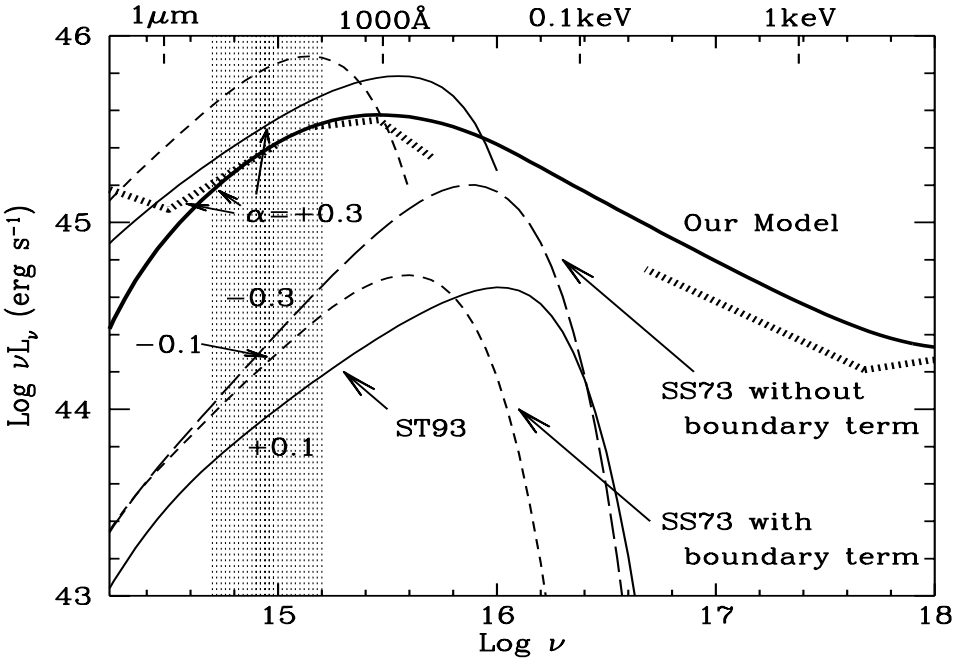

FIG. 3.— Spectra of various models with optical spectral indices α ($L_\nu \propto \nu^{-\alpha}$). The shaded area inndicates the relevant waveband, 1500–5000 Å. Thick solid and dotted lines have the same meanings as in Fig. 2a. Spectra of the standard disks [Shakura & Sunyaev 1973 (SS73), i.e., eq. 4] are shown as the short-dashed lines as in Fig. 2a. A long-dashed one is calculated through eq. 4 without inner boundary term (the last term in eq. 4). Finally, thin solid curves are obtained by radial integrations of ST93 model (i.e., no corona). Lower three calculations are made for $M_{\rm BH} = 10^8 M_\odot$ and $\dot{M} = L_{\rm Edd}/c^2$ at $3 < R < 1000 R_g$, while upper two curves are for $M_{\rm BH} = 3\,10^9 M_\odot$ and $\dot{M} = 0.5\,L_{\rm Edd}/c^2$ at the same radii.

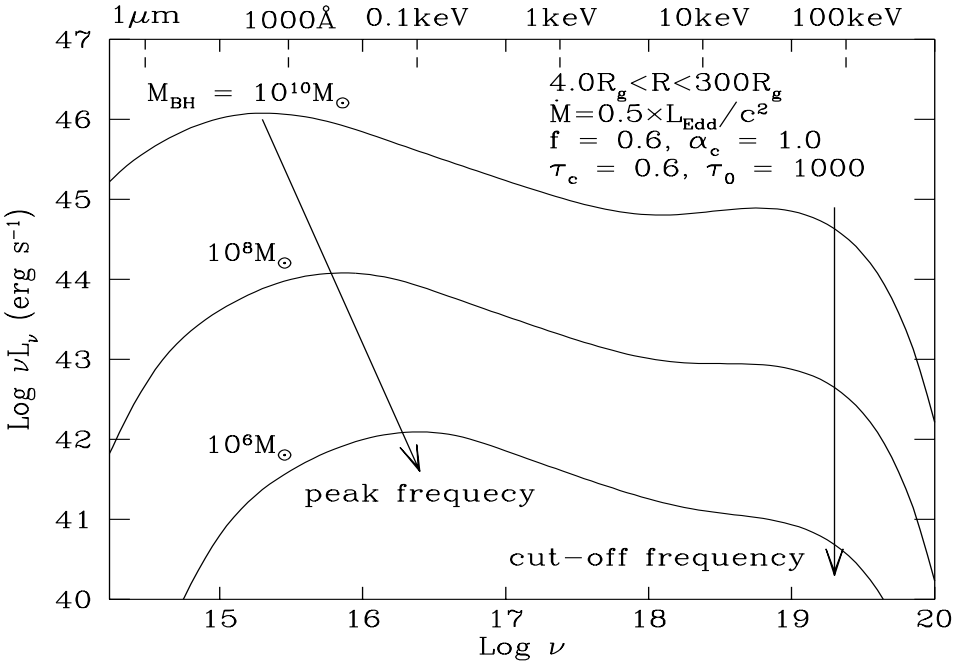

FIG. 4.— Black-hole mass dependence of the emergent spectra with a fixed ratio of $\dot{M}$ to $L_{\rm Edd}$. Parameters used here are the same as those of Fig. 2a and 2b. The cut-off frequency of the hard X-ray (reflecting the coronal electron temperature) and X-ray spectral slopes are insensitive to the black-hole mass, while the peak frequency of the big blue bump is sensitive to the mass.

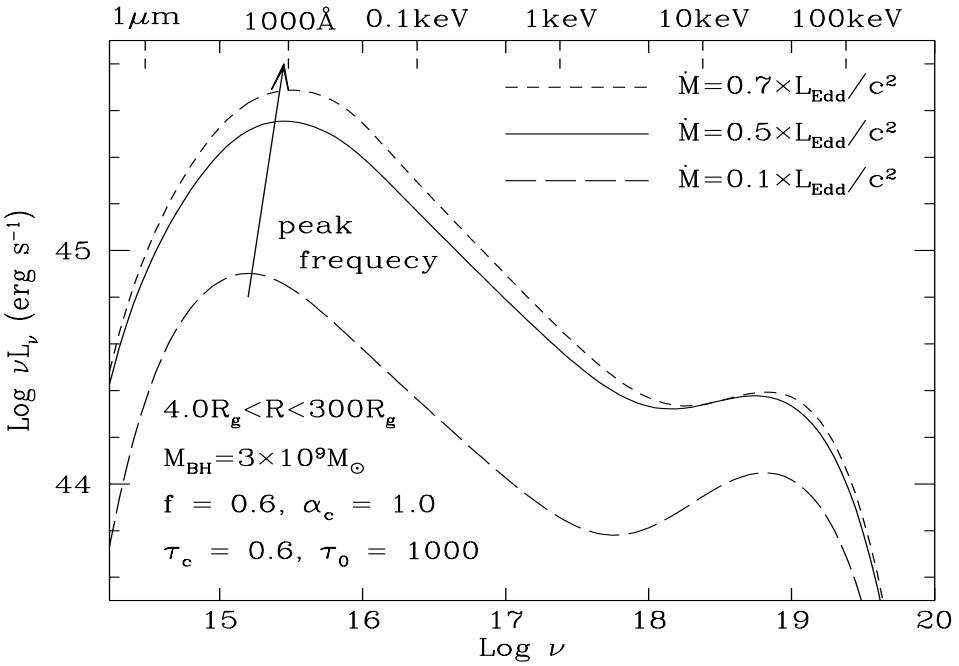

FIG. 5.— Accretion-rate dependence of the emergent spectra with a fixed black-hole mass ($M_{\rm BH} = 3 \times 10^9 M_\odot$).

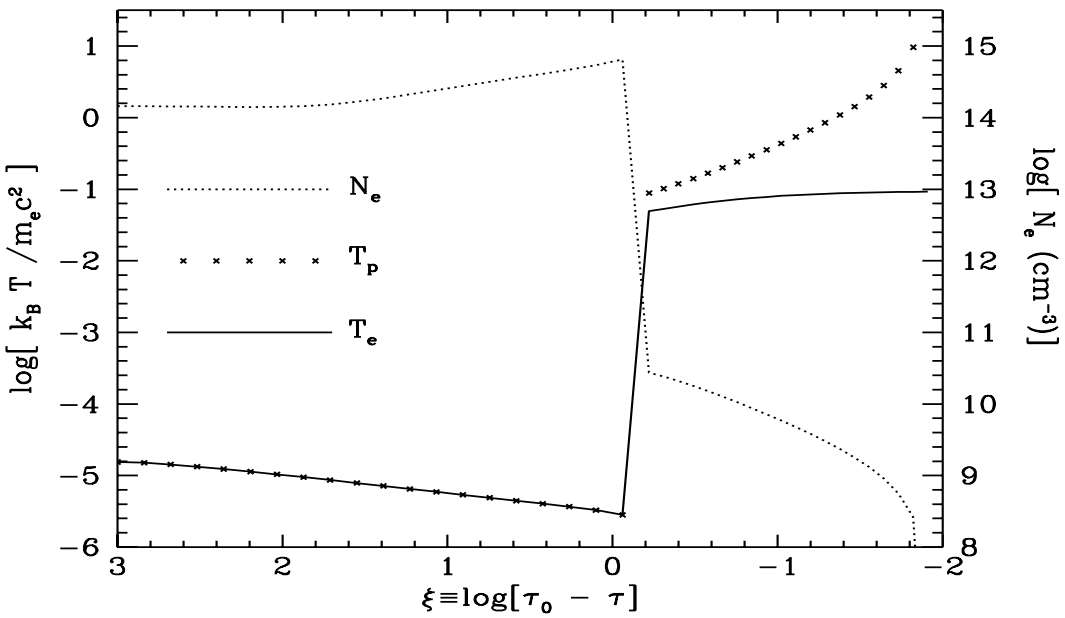

FIG. 6.— Vertical structure of the matter density (dotted line), proton temperature (crosses), and electron temperature (solid line). The mid-plane of the disk is located at ξ of 3, and the boundary between the disk and corona is at $\xi \sim -0.2$. It turns out that the height of the boundary measured from the mid-plane is 0.03 $R_{\rm g}$, and that of the surface of the corona (at ξ of -2) is 0.3 $R_{\rm g}$. Note that $k_{\rm B}T/m_{\rm e}c^2 = 1$ corresponds to $T \simeq 5\ 10^9$ K ($\simeq 500$ keV).